

A Priori Generalizability Estimate for a CNN

Cito Balsells^{1,2}

Beatrice Riviere¹

David Fuentes²

¹ Department of Computational Applied Mathematics and Operations Research, The Kennedy Institute, Rice University, 6100 Main St, Houston, TX, 77005, USA

² Department of Imaging Physics, The University of Texas MD Anderson Cancer Center, 1515 Holcombe Blvd, Houston, TX, 77030, USA

Abstract

We formulate truncated singular value decompositions of entire convolutional neural networks. We demonstrate the computed left and right singular vectors are useful in identifying which images the convolutional neural network is likely to perform poorly on. To create this diagnostic tool, we define two metrics: the Right Projection Ratio and the Left Projection Ratio. The Right (Left) Projection Ratio evaluates the fidelity of the projection of an image (label) onto the computed right (left) singular vectors. We observe that both ratios are able to identify the presence of class imbalance for an image classification problem. Additionally, the Right Projection Ratio, which only requires unlabeled data, is found to be correlated to the model's performance when applied to image segmentation. This suggests the Right Projection Ratio could be a useful metric to estimate how likely the model is to perform well on a sample.

Introduction

There has been a growing trend of increasing the compute power available to machine learning models in an effort to improve model performance. This can be seen with estimates that the total compute power of all NVIDIA chips has doubled every 10 months since 2019 [Epoch AI \[2024\]](#). However, this approach is generally only accessible to a handful of large technology companies. It is not practical, nor potentially even feasible, for every organization to increase their compute power. For resource constrained settings, it is therefore crucial to find ways to maximize model performance with respect to the available resources. There are two popular ways to accomplish this: parameter reduction and identifying a coreset for training.

While our research is more applicable to finding a coreset, we discuss parameter reduction since our methods use topics related to it. We will analyze a specific class of machine learning

model referred to as a convolutional neural network (CNN) that is commonly used for image classification and image segmentation. A common approach to parameter reduction is to compute low rank approximations for *specific weight tensors* in a model to reduce memory usage. This has been shown to effectively reduce memory usage and speed up model inference while maintaining comparable performance [Denton et al. \[2014\]](#); [Jaderberg et al. \[2014\]](#). In [Denton et al. \[2014\]](#), the authors demonstrate a $2\times$ speedup within the convolutional layers by replacing each convolution kernel with a low rank approximation obtained by a higher-order singular value decomposition (SVD).

Our contribution is in computing the truncated SVD for *the entire CNN* and demonstrating that it can serve as a useful diagnostic tool. To our knowledge, computing the SVD of a whole CNN is a novel application. We will show that this truncated SVD can identify which unlabeled images the model will likely perform well or poorly on. This is accomplished by evaluating the fidelity of the image and its projection onto the right singular vectors. This can then be used to assess whether or not there is bias in the model. There are existing diagnostic tools that assess models; however, they evaluate models component by component. For example, WeightWatcher from [Martin and Mahoney \[2018\]](#) performs a number of tasks including quantifying how well or poorly trained a layer is, finding outliers in the training set, and making test set predictions with or without training or testing data. This is accomplished by looking at *individual weight matrices* in dense neural networks and analyzing their spectrum of eigenvalues.

In general settings, it is only possible to compute the truncated SVD of a CNN with implicit methods. This requires an operator that performs the transpose or adjoint of the CNN. This operator, which we refer to as the Adjoint CNN, is defined and constructed in [Section 1.1](#). In [Section 1.2](#) we detail how we compute the SVD and how it is used to evaluate the fidelity of projections. Then in [Section 1.3](#) and [Section 1.4](#) we present the methods behind our experiments on two different datasets. Following the methods, we present our results in [Section 2](#) with our interpretation of the results in [Section 3](#).

Primary contributions of this paper:

1. Theoretical and empirical proof that the adjoint of the matrix associated with a CNN can be interpreted as a closely related CNN,
2. Demonstration on two datasets that metrics derived from the SVD, the Right and Left Projection Ratios, can identify when a CNN is likely to perform well or poor.

1 Methods

We provide a general overview for how we compute the SVD of an arbitrary CNN. The CNNs we study are compositions of: convolution (with no bias), downsampling, upsampling, ReLU

activation, and skip connections.

Let $X \in \mathbb{R}^{m \times n \times d \times c_{in}}$ be a tensor which represents data with three spatial dimensions, $m \times n \times d$, and c_{in} channels. For example, X could represent a 3D MRI scan ($m = n = d = 128$) with four channels ($c_{in} = 4$). Then $\mathcal{F}_\theta : \mathbb{R}^{m \times n \times d \times c_{in}} \rightarrow \mathbb{R}^{m \times n \times d \times c_{out}}$ represents a CNN that takes a 3D tensor, X , and produces a voxel-wise segmentation with c_{out} possible classes. We define the operator, $\text{vec}()$, that ‘flattens’ a tensor into a vector such that for $x = \text{vec}(X) \in \mathbb{R}^{mndc_{in}}$, we have $x_{j+ni+mnk+mndc} = X_{i,j,k,c}$. We likewise define the operator, $\text{tensor}()$, which reverses this operation, ie $\text{tensor}(x) = X$. It is possible to write down an input dependent matrix $A[x] \in \mathbb{R}^{mndc_{out} \times mndc_{in}}$ such that,

$$A[x]x = \text{vec}(\mathcal{F}_\theta(X)). \quad (1)$$

We direct readers to [Balestrierio and Baraniuk \[2018\]](#) for a precise construction. We will refer to the left hand side as the ‘matrix representation’ which acts over vectors. We will refer to the right hand side as the ‘tensor representation’ which acts over tensors. In order to have a fixed matrix to analyze, we compute the SVD of $A[x]$ for *each image* x .

While it is theoretically possible to explicitly create the matrix, it may not be practical. Therefore, we focus on Krylov subspace methods to compute the SVD since these methods only require operators that compute the products $A[x]y$ and $A^T[x]z$ for any $y \in \mathbb{R}^{mndc_{in}}$ and $z \in \mathbb{R}^{mndc_{out}}$. Our primary theoretical contribution is in proving that the matrix, $A^T[x]$, which we refer to as the adjoint matrix, corresponds to a closely related CNN, which we refer to as the Adjoint CNN, where,

$$\begin{aligned} A^T[x]x &= \text{vec}(\mathcal{G}_\theta(X)), \\ \mathcal{G}_\theta : \mathbb{R}^{m \times n \times d \times c_{out}} &\rightarrow \mathbb{R}^{m \times n \times d \times c_{in}}. \end{aligned} \quad (2)$$

We outline our theoretical construction of the Adjoint CNN in Section 1.1. Following this in Section 1.2, we discuss how we implement SVD solvers and how the computed singular triplets can be used to create a ‘low rank’ approximation of the CNN. Then in Section 1.3 we present the methods using the MNIST dataset to verify properties of the SVD. Next, in Section 1.4 we present the methods behind our analysis of CNNs applied to tumor segmentation with the BraTS dataset.

1.1 Theory to Construct the Adjoint CNN

Each operation in a CNN can be written down as a (possibly input-dependent) matrix. This enables us to write down,

$$\mathcal{F}_\theta(X) = F_L \circ F_{L-1} \circ \dots \circ F_0(X) \leftrightarrow A[x] = A_L[x]A_{L-1}[x] \dots A_0[x], \quad (3)$$

where each F_ℓ corresponds to one operation. Therefore, we can compute the adjoint matrix, and consequently the adjoint CNN, by identifying what $A_\ell^T[\cdot]$ performs for each operation. To provide an example, we will analyze downsampling and upsampling. Then we will state the results for the other operations in Table 1 and direct the reader to the supplemental information for their formal proofs.

The CNNs in this paper use sumpooling for downsampling and nearest neighbor for upsampling. This choice was made for two reasons: the associated matrices are input independent and are adjoint to each other. However, it is possible to use maxpooling instead at the cost of introducing more input-dependent components. Before defining sumpooling and nearest neighbor upsampling, we define the region associated with a voxel.

Definition 1 (Region). *Given a voxel located at $(i, j, k) \in [m] \times [n] \times [d]$,¹ its (tensor) region is:*

$$R_{(i,j,k)} = \{(2i + \delta_0, 2j + \delta_1, 2k + \delta_2 | \delta_0, \delta_1, \delta_2 \in \{0, 1\}\}, \\ \subset [2m] \times [2n] \times [2d].$$

For the corresponding flattened index, $p = j + ni + mnk$, we overload the $\text{vec}(\cdot)$ function to define its (vector) region as:

$$R_{(p)} = \text{vec}(R_{(i,j,k)}), \\ = \{\hat{j} + n\hat{i} + mn\hat{k} | (\hat{i}, \hat{j}, \hat{k}) \in R_{(i,j,k)}\}.$$

Assume that m , n , and d are all even. Then, sumpooling is defined as:

$$\Pi_\downarrow : \mathbb{R}^{m \times n \times d} \rightarrow \mathbb{R}^{\frac{m}{2} \times \frac{n}{2} \times \frac{d}{2}}, \\ [\Pi_\downarrow(X)]_{i,j,k} = \sum_{(s,t,u) \in R_{(i,j,k)}} X_{s,t,u}.$$

Lemma 1. *The sumpooling operator $\Pi_\downarrow : \mathbb{R}^{m \times n \times d} \rightarrow \mathbb{R}^{\frac{m}{2} \times \frac{n}{2} \times \frac{d}{2}}$ can be expressed as an input independent matrix, $A_\downarrow \in \mathbb{R}^{\frac{mnd}{8} \times mnd}$. Let $e_q \in \mathbb{R}^{mnd}$ represent the q th canonical basis vector. Then the matrix has rows defined as,*

$$[A_\downarrow]_{p,\cdot} = \sum_{q \in R_{(p)}} e_q^T,$$

where,

$$A_\downarrow x = \text{vec}(\Pi_\downarrow(X)).$$

¹ $[m] = \{0, 1, \dots, m-1\}$

Nearest neighbor upsampling is a closely related operation defined as:

$$\begin{aligned}\Pi_{\uparrow} : \mathbb{R}^{m \times n \times d} &\rightarrow \mathbb{R}^{2m \times 2n \times 2d} \\ [\Pi_{\uparrow}(X)]_{s,t,u} &= X_{i,j,k}, \quad (s,t,u) \in R_{(i,j,k)}.\end{aligned}$$

Lemma 2. *The nearest neighbor upsampling operator $\Pi_{\uparrow} : \mathbb{R}^{m \times n \times d} \rightarrow \mathbb{R}^{2m \times 2n \times 2d}$ can be expressed as an input independent matrix, $A_{\uparrow} \in \mathbb{R}^{8mnd \times mnd}$, with columns defined as,*

$$[A_{\uparrow}]_{\cdot,p} = \sum_{q \in R(p)} e_q,$$

such that,

$$A_{\uparrow}x = \text{vec}(\Pi_{\uparrow}(X)).$$

Lemma 3. *Assume m, n, d even. Sumpooling, $\Pi_{\downarrow} : \mathbb{R}^{m \times n \times d} \rightarrow \mathbb{R}^{\frac{m}{2} \times \frac{n}{2} \times \frac{d}{2}}$, and nearest neighbor upsampling, $\Pi_{\uparrow} : \mathbb{R}^{\frac{m}{2} \times \frac{n}{2} \times \frac{d}{2}} \rightarrow \mathbb{R}^{m \times n \times d}$, are adjoint to each other.*

Proof - Use Lemma 1, and consider the p th column of A_{\downarrow}^T :

$$\begin{aligned}[A_{\downarrow}^T]_{\cdot,p} &= [[A_{\downarrow}]_{p,\cdot}]^T \\ &= \left(\sum_{q \in R(p)} e_q^T \right)^T = [A_{\uparrow}]_{\cdot,p}\end{aligned}$$

Operation	Example	Adjoint	Example
Sumpooling	$\begin{bmatrix} 1 & -5 \\ 3 & 2 \end{bmatrix} \mapsto [1]$	Nearest Neighbor Upsampling	$[1] \mapsto \begin{bmatrix} 1 & 1 \\ 1 & 1 \end{bmatrix}$
Maxpooling	$\begin{bmatrix} 1 & -5 \\ \mathbf{3} & 2 \end{bmatrix} \mapsto [3]$	Zero stuffing	$[3] \mapsto \begin{bmatrix} 0 & 0 \\ \mathbf{3} & 0 \end{bmatrix}$
Convolution	$\mathcal{C} \in \mathbb{R}^{3 \times 3 \times 3 \times \alpha \times \beta}$	Convolution	$\tilde{\mathcal{C}} \in \mathbb{R}^{3 \times 3 \times 3 \times \beta \times \alpha}$
ReLU	$\begin{bmatrix} 1 & -5 \\ 3 & 2 \end{bmatrix} \mapsto \begin{bmatrix} 1 & 0 \\ 3 & 2 \end{bmatrix}$	‘Frozen’ ReLU	$\begin{bmatrix} a & b \\ c & d \end{bmatrix} \mapsto \begin{bmatrix} a & 0 \\ c & d \end{bmatrix}$
Skip Connection	$x \mapsto \begin{bmatrix} Mx \\ x \end{bmatrix}$	Residual Connection	$\begin{bmatrix} y_{\alpha} \\ y_{\beta} \end{bmatrix} \mapsto My_{\alpha} + y_{\beta}$

Table 1: Summary of CNN operations and the operation associated with their adjoint.

Using Table 1 and Equation 3, we may construct the Adjoint CNN:

$$\begin{aligned}A^T[x] &= A_0^T[x] \dots A_{L-1}^T[x] A_L^T[x] \\ &\leftrightarrow \\ \mathcal{G}_{\theta}(X) &= G_L \circ G_{L-1} \circ \dots \circ G_0(X).\end{aligned}\tag{4}$$

1.2 Implementation of Solver and its Utility

We first present how we use the SVD to create a ‘low rank CNN’. Assume $A[x]$ has rank r and SVD:

$$A[x] = \sum_{i=1}^r \sigma_i[x] u_i[x] v_i^T[x]. \quad (5)$$

Traditionally, the CNN generates class probabilities by computing:

$$\widehat{P}(X) = \sigma_{\text{softmax}}(\mathcal{F}_\theta(X)) \in \mathbb{R}^{m \times n \times d \times c_{out}}, \quad (6)$$

where the final predicted segmentation is:

$$\begin{aligned} P(X) &\in \mathbb{R}^{m \times n \times d}, \\ [P(X)]_{i,j,k} &= \arg \max_c [\widehat{P}(X)]_{i,j,k,c} \in \{0, 1, \dots, c_{out} - 1\}. \end{aligned} \quad (7)$$

Notice that the CNN model class probabilities could be equivalently computed as:

$$\begin{aligned} \widehat{P}(X) &= \sigma_{\text{softmax}}(\mathcal{F}_\theta(X)) \\ &= \sigma_{\text{softmax}}(\text{tensor}(A[x]x)) \\ &= \sigma_{\text{softmax}}\left(\text{tensor}\left(\sum_{i=1}^r \sigma_i[x] u_i[x] v_i^T[x] x\right)\right). \end{aligned}$$

This insight allows us to compute the prediction from the ‘ k rank CNN’ by using the k rank approximation of $A[x]$, denoted $A_k[x]$, as:

$$\begin{aligned} \widehat{P}_k(X) &= \sigma_{\text{softmax}}\left(\text{tensor}\left(\sum_{i=1}^k \sigma_i[x] u_i[x] v_i^T[x] x\right)\right), \\ &= \sigma_{\text{softmax}}(\text{tensor}(A_k[x]x)). \end{aligned} \quad (8)$$

We use the Python adaptation of SLEPC [Dalcin et al. \[2011\]](#); [Hernandez et al. \[2005\]](#) to compute the SVD. We use its default “cross” solver. This solver computes the eigenvalue decomposition of $H(A) = A^T A = V \Lambda V^{-1}$ using an implicit Krylov-Schur method to compute the singular values and right singular vectors. Then it computes the left singular vectors by normalizing Av_j . SLEPC evaluates the error of its approximation by computing the residual,

$$\|r\|_2 = \left(\|A\tilde{v} - \tilde{\sigma}\tilde{u}\|_2^2 + \|A^T\tilde{u} - \tilde{\sigma}\tilde{v}\|_2^2\right)^{\frac{1}{2}},$$

where $(\tilde{\sigma}, \tilde{u}, \tilde{v})$ represents the solver’s estimate for an arbitrary singular triplet. We set SLEPc to consider the relative error.

In addition to computing the rank k CNN prediction using Equation (8), we are interested in the subspaces formed by the span of the computed singular vectors. Recall the singular vectors are orthonormal and hence we can consider the projection of a sample, x , onto the span of the right singular vectors:

$$V_k[x]V_k^T[x]x, \quad V_k[x] = [v_1[x] \dots v_k[x]]. \quad (9)$$

We use the following ratio, which we call the Right Projection Ratio (RPR), to evaluate how well x is approximated by its projection onto the subspace spanned by the k right singular vectors:

$$\text{RPR}(x; k) = \frac{\|V_k[x]V_k^T[x]x\|_2^2}{\|x\|_2^2} \in [0, 1], \quad (10)$$

where,

$$\text{RPR}(x; k) = \begin{cases} 1, & x \in R(A_k^T[x]) \\ 0, & x \in N(A_k[x]) \supset N(A[x]) \end{cases}$$

We may use this ratio as an estimate for how close the input image is to the nullspace of the CNN. To illustrate why an RPR close to zero is problematic, assume $x \in N(A[x])$. Then,

$$x \in N(A[x]) \implies \mathcal{F}_\theta(X) \equiv 0 \in \mathbb{R}^{m \times n \times d \times c_{out}}. \quad (11)$$

To focus on an arbitrary voxel, (i, j, k) , notice that the class probabilities are,

$$\begin{aligned} [\hat{P}(X)]_{i,j,k,\cdot} &= [\sigma_{\text{softmax}}(0)]_{i,j,k,\cdot} \\ &= \left[\frac{1}{c_{out}}, \dots, \frac{1}{c_{out}} \right]. \end{aligned} \quad (12)$$

This means that each class is equally likely to be selected and represents a high degree of model uncertainty. Additionally, this could introduce algorithmic bias. For example, the argmax functions in both NumPy and PyTorch always return the indices of the first occurrence when there are multiple occurrences of the maximum value.

It is a little more involved to evaluate a similar ratio using the left singular vectors. For this discussion, we consider a CNN tasked with image classification. We need to construct a mapping from the space of possible labels to the raw logits output space. Assume x has label $\ell \in \{0, 1, \dots, c_{out} - 1\}$. From Equation (7), we see that we need to pick $y \in \mathbb{R}^{c_{out}}$ such that $\ell = \arg \max(y)$. Once a mapping is created, we can compute the Left Projection Ratio (LPR) which evaluates how well the projection of y onto the k left singular vectors approximates y :

$$\text{LPR}(y; k) = \frac{||U_k[x]U_k^T[x]y||_2^2}{||y||_2^2} \in [0, 1]. \quad (13)$$

Similar to the RPR, we have,

$$\text{LPR}(y; k) = \begin{cases} 1, & y \in R(A_k[x]) \subset R(A[x]) \\ 0, & y \in N(A_k^T[x]) \supset N(A^T[x]) \end{cases}$$

1.3 Image Classification

The MNIST dataset consists of 60000 training images and 10000 testing images. Each image, $X \in \mathbb{R}^{28 \times 28}$, belongs to exactly one class out of 10 possible. Therefore, the matrix representation of this problem has,

$$A[x] \in \mathbb{R}^{10 \times 28^2}.$$

With an upper bound known for the rank, we compute the rank $k \in \{1, 2, \dots, 10\}$ approximation for each image.

The CNN architecture consists of the following layers:

- Convolution with kernel size 5×5 , 32 filters, zero padding, followed by ReLU,
- Sumpooling,
- Convolution with kernel size 5×5 , 64 filters, zero padding, followed by ReLU,
- Sumpooling,
- A linear mapping to 512 nodes followed by ReLU,
- A linear mapping to 256 nodes followed by ReLU,
- A linear mapping to 10 nodes,
- Softmax final activation.

We use a batch size of 32, stochastic gradient descent with cross entropy loss, a learning rate of 3×10^{-3} , and we train for 50 epochs.

We use the default SVD solver from SLEPc4py and set the tolerance on the relative error of the solver to 10^{-5} .

As an additional experiment to determine if the SVD can be used to identify bias in the model, we train a second CNN on a heavily unbalanced training set. For the unbalanced training set, we remove 99% of the images belonging to digits $\{1, 9\}$.

In order to evaluate the LPR, we map the label $\ell \in \{0, 1, \dots, 9\}$ to $y \in \mathbb{R}^{10}$ where,

$$[y(\ell)]_i = \begin{cases} 2, & i = \ell \\ -2, & i \neq \ell \end{cases}$$

This choice was made by observing that after applying softmax, we have:

$$\sigma_{\text{softmax}}(y(\ell))_i \approx \begin{cases} 0.86, & i = \ell \\ 0.016, & i \neq \ell \end{cases}$$

Broadly interpreted, this mapping is one way to check if the model can predict with 86% certainty the correct class. This selection was motivated by observing that the rank 1 Matrix Representation assigned an average probability around 0.8 when it predicted correctly and that the Tensor Representation assigned an average probability nearly equal to 1 for its correct predictions.

1.4 Image Segmentation

To consider a more practical application where it would be infeasible to compute the compact SVD, we demonstrate as a proof of concept how to analyze a CNN trained to segment brain tumors. We use the Brain and Tumor Segmentation 2020 dataset from [Menze and et al. \[2015\]](#); [Bakas and et al. \[2018, 2017\]](#) which consists of 369 3D multi-modal MRI scans with multi-label tumor segmentation masks. We combine the tumor masks to consider binary tumor segmentation. We use the MIST framework from [Celaya et al. \[2024\]](#); [Celaya \[2025\]](#) to preprocess the data and perform five fold cross validation with a general UNet based architecture:

- Operates on patches of size $(128, 128, 128)$,
 - That is, $\mathcal{F}_\theta : \mathbb{R}^{128 \times 128 \times 128 \times 4} \rightarrow \mathbb{R}^{128 \times 128 \times 128 \times 2}$
- Depth 5,
- Each convolutional layer consists of two convolution+ReLU pairs,
 - We use the Pocket Paradigm from [Celaya et al. \[2024\]](#) and fix the number of convolution filters to 32

- Sumpooling,
- Nearest neighbor upsampling,
- Skip connections

We use a batch size of 2, the Adam optimizer with L2 relaxed dice loss, a learning rate of 3×10^{-4} , and train for 1000 epochs. The validation set was used to prevent overfitting and select the best model.

We use the default SVD solver from SLEPc4py and set the tolerance on the relative error to 10^{-4} . We chose to compute 10 singular triplets.

For both training and computing the SVD, we used Monai’s sliding window inference function to stitch together the full prediction from patches.

2 Results

In Section 2.1 we present the image classification results with the MNIST dataset. In Section 2.2, we present our findings from the segmentation problem with the BraTS dataset.

2.1 MNIST Classification

We evaluated both CNNs, referred to as the ‘Tensor Model’, on the test set. The well balanced Tensor Model correctly labeled 9864 images giving it an accuracy of 0.9864 and the unbalanced Tensor Model correctly labeled 9329 images giving it an accuracy 0.9329. It is important to highlight that the balanced rank 10 CNN also had an accuracy of 0.9864 and failed on the same 136 images as the balanced Tensor Model. Likewise, the unbalanced rank 10 CNN failed on the same 671 images as the unbalanced Tensor Model. In Figure 1 we compare the rank k CNN accuracy to the Tensor Model stratified over each digit.

In order to have class specific information, we look at the distribution of the projection ratios with respect to each digit. We present the distribution at ranks 2, 3, 4, 5, 6 for the RPR in Figure 2 and for the LPR in Figure 3.

Finally, included in the Supplemental Information are a few visual examples of the computed singular vectors and the associated projections.

2.2 BraTS Segmentation

The mean test dice score for the Tensor Representation was 0.9067. In Figure 4 we present the Tensor CNN dice score against its RPR for every volume. This is summarized in Table 2 where we report the mean dice score for images with RPR within certain ranges.

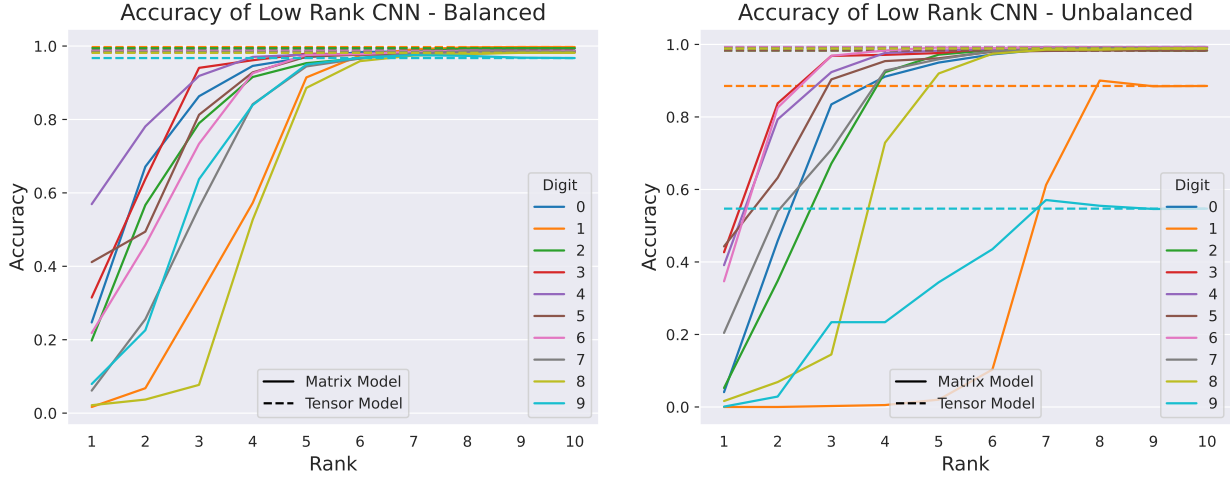


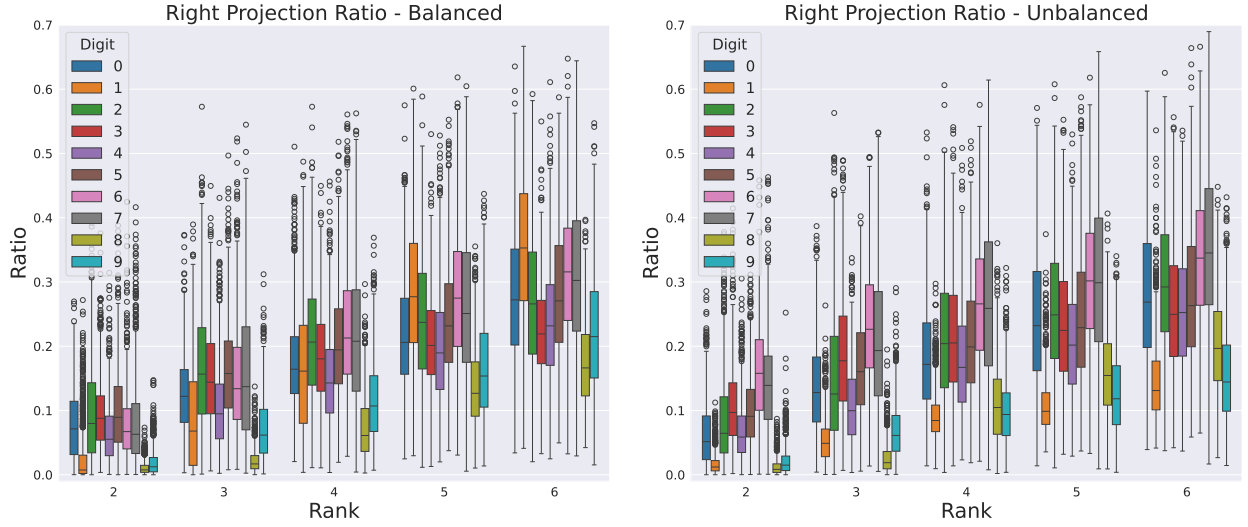
Figure 1: Evaluating the digit specific accuracy of the balanced (left) and unbalanced (right) rank k CNN.

RPR Quantile	Mean Dice Score
Below 10%	0.7728
Within 10 – 50%	0.8979
Within 50 – 90%	0.9375
Above 90%	0.9522
Entire Set	0.9067

Table 2: Breakdown of Mean Dice Score by RPR for full five fold cross validation (369 volumes).

3 Discussion

We evaluated our SVD-based approach on the MNIST image classification problem since it would be feasible to compute the compact SVD and verify that what we computed as various rank approximations to the CNN does indeed behave like an SVD. The first validating observation was that for both the CNN trained on the balanced dataset and the CNN trained on the unbalanced dataset, there was steady convergence of the low rank accuracy to the Tensor Model accuracy as shown at the digit level in Figure 1. This behavior is consistent with the fact that $A_k[x]$ converges to $A[x]$ as k tends to the full rank r . Additionally, the rank 10 matrix model and the Tensor Model failed on the same images which offers empirical support that the computed rank 10 Matrix Representation, $A_{10}[\cdot]$, is fundamentally equivalent to the Tensor Representation, $\mathcal{F}_\theta(\cdot)$.

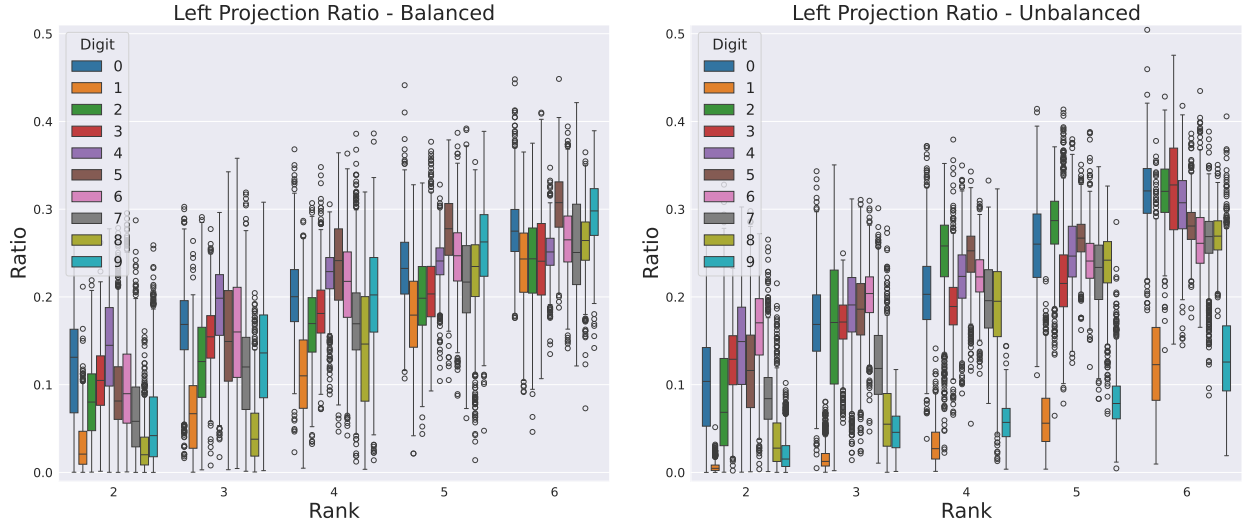


(a) For the CNN trained on the balanced dataset. (b) For the CNN trained on the unbalanced dataset.

Figure 2: Boxplot showing how the RPR changes for each digit as the rank increases. Using the RPRs from the balanced model as a baseline, we observe that digit 1 deviates the most for the unbalanced dataset. With its significantly stunted RPR, this can be interpreted as images depicting the digit 1 belonging more to the nullspace of the CNN. Additionally, the RPR for digit 9, which was generally above digit 8 for the balanced experiment, drops below digit 8 for the unbalanced experiment. By evaluating proximity to the nullspace with the RPR, we can identify digits $\{1, 9\}$ as candidates of poor model performance for the unbalanced experiment.

The second validating observation was that the RPR and LPR monotonically increased with the rank. At rank 10, the LPR was exactly 1. This was expected since the dimension of the label space was 10 and hence $U_{10}[x]$ formed an orthonormal basis that spanned the entire space.

We found that the projection ratios were able to identify the class imbalance between the two CNNs. Looking at the RPR for the balanced CNN in Figure 2a as a baseline, we saw that digit 8 was the slowest digit to improve. Comparing this against the RPR for the unbalanced CNN, we noticed that digits $\{1, 8, 9\}$ were the slowest to improve. Digit 8 can be seen as an artifact since it was included in both models. This suggests that the RPR provides a means to estimate whether or not there is bias within a model as was the case here. This signal was even more clear for the LPR in Figure 3 where digits $\{1, 9\}$ had significantly smaller ratios.



(a) For the CNN trained on the balanced dataset. (b) For the CNN trained on the unbalanced dataset.

Figure 3: Boxplot showing how the LPR changes for each digit as the rank increases. When the training set is unbalanced, digits $\{1, 9\}$ consistently have the lowest LPRs. Referring back to Section 1.2, we recognize that this means these digits are not well represented in the range of the CNN. This offers improved interpretability for why the CNN trained on the unbalanced dataset performed worse than the CNN trained on the balanced dataset.

One might be inclined to explain the poor performance of the unbalanced CNN on digits $\{1, 9\}$ in Figure 1 as a lack of training. With our approach, our explanation is that the CNN was unable to sufficiently adapt its range and null space to properly accommodate the missing digits. That is, the lack of training meant that the digits were not as easy for the model to express. This would require more singular vectors, corresponding to less important features of the CNN, to improve the projection ratios.

This correlation between the RPR and the CNN performance was additionally observed for tumor segmentation with rank 10 approximations. When we ordered the test set by the RPR of the volume, we found that the volumes that belonged to the top 10% quantile had an average dice score of 0.9522 with none below 0.9. Conversely, the volumes that belonged to the bottom 10% quantile had an average dice score of 0.7728. This demonstrates that the RPR could be used as an estimate for the dice score.

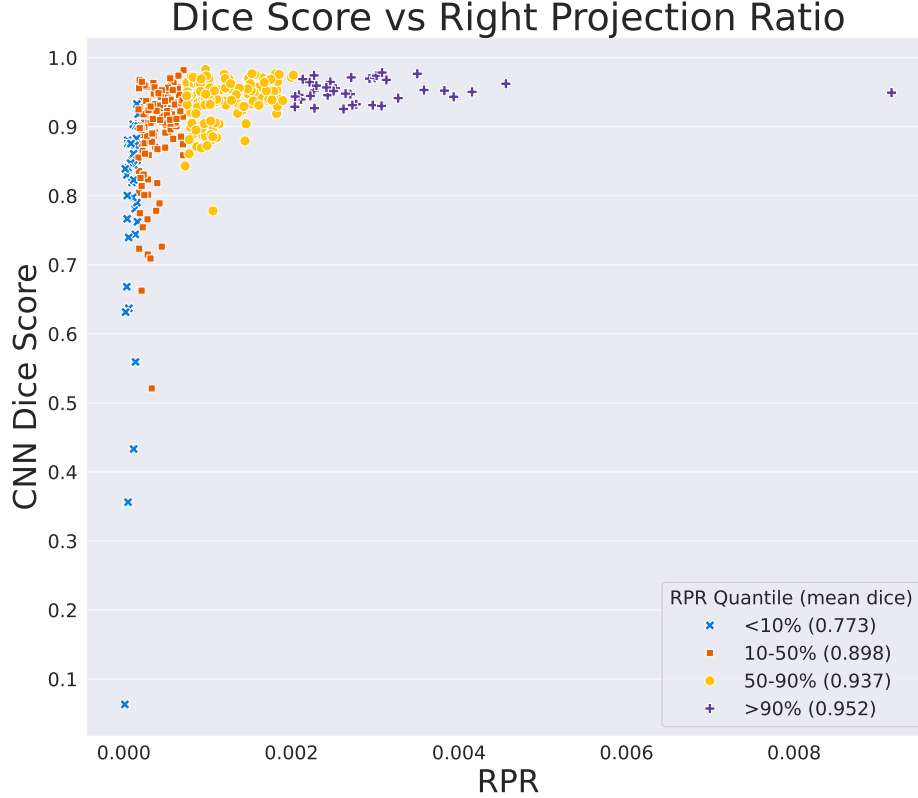


Figure 4: The RPR is calculated using the 10 right singular vectors corresponding to the 10 largest singular values. The ‘CNN Dice Score’ is the dice score from the Tensor Representation of the CNN. Test set contains 369 volumes.

4 Conclusion

We introduced a methodology for computing the singular value decomposition of a convolutional neural network. The utility of this computation is in its ability to quantify to what degree an image, a segmentation mask, or a classification label belongs to the range and nullspace of the CNN. This was accomplished by defining the Right and Left Projection Ratio that use the right and left singular vectors from the truncated SVD respectively. We observed that the projection ratios were able to identify class imbalance between two models trained for classification with the MNIST dataset.

Additionally, we observed that the Right Projection Ratio can estimate the quality of a segmentation mask for a more challenging task like tumor segmentation. This could be useful in active learning problems where it is desirable to select a batch of images from an

unlabeled pool that the CNN would likely perform poorly on. Alternatively, the RPR could be useful in a recommender system where the goal is to select an image that maximizes some objective where the true label or segmentation is unknown.

Acknowledgments

This research was partially funded by a training fellowship from the Keck Center of the Gulf Coast Consortia, on the Training Program in Biomedical Informatics, National Library of Medicine (NLM), PI Lydia Kavraki, grant number: T15LM007093-30.

This work was partly supported by the Tumor Measurement Initiative through the MD Anderson Strategic Initiative Development Program (STRIDE) and QIAC Partnership in Research (QPR) Program. NIH support under R01CA195524, and NSF support under Awards NSF-2111147, 2231482, 2111459 is gratefully acknowledged.

References

- S Bakas and et al. Advancing the cancer genome atlas glioma mri collections with expert segmentation labels and radiomic features. *Scientific Data*, 4(1):170117, 2017. ISSN 2052-4463. doi: 10.1038/sdata.2017.117. URL <https://doi.org/10.1038/sdata.2017.117>.
- S. Bakas and et al. Identifying the best machine learning algorithms for brain tumor segmentation, progression assessment, and overall survival prediction in the brats challenge. *arXiv preprint arXiv:1811.02629*, 2018.
- Randall Balestriero and Richard Baraniuk. Mad max: Affine spline insights into deep learning. *Proceedings of the IEEE*, 2018. URL <https://arxiv.org/abs/1805.06576>.
- Adrian Celaya. Medical imaging segmentation toolkit. *GitHub repository*, 2025. URL <https://github.com/mist-medical/MIST>.
- Adrian Celaya, Evan Lim, Rachel Glenn, Brayden Mi, Alex Balsells, Dawid Schellingerhout, Tucker Netherton, Caroline Chung, Beatrice Riviere, and David Fuentes. Mist: A simple and scalable end-to-end 3d medical imaging segmentation framework, 2024. URL <https://arxiv.org/abs/2407.21343>.
- Lisandro D. Dalcin, Rodrigo R. Paz, Pablo A. Kler, and Alejandro Cosimo. Parallel distributed computing using python. *Advances in Water Resources*, 34(9):1124–1139, 2011. ISSN 0309-1708. doi: <https://doi.org/10.1016/j.advwatres.2011.04.013>. URL <https://www.sciencedirect.com/science/article/pii/S0309170811000777>. New Computational Methods and Software Tools.

- Remi Denton, Wojciech Zaremba, Joan Bruna, Yann LeCun, and Rob Fergus. Exploiting linear structure within convolutional networks for efficient evaluation, 2014. URL <https://arxiv.org/abs/1404.0736>.
- Epoch AI. Data on machine learning hardware, 2024. URL <https://epoch.ai/data/machine-learning-hardware>. Accessed: 2025-02-16.
- Vicente Hernandez, Jose E. Roman, and Vicente Vidal. Slepnc: A scalable and flexible toolkit for the solution of eigenvalue problems. *ACM Trans. Math. Softw.*, 31(3):351–362, sep 2005. ISSN 0098-3500. doi: 10.1145/1089014.1089019. URL <https://doi.org/10.1145/1089014.1089019>.
- Max Jaderberg, Andrea Vedaldi, and Andrew Zisserman. Speeding up convolutional neural networks with low rank expansions, 2014. URL <https://arxiv.org/abs/1405.3866>.
- Charles H. Martin and Michael W. Mahoney. Implicit self-regularization in deep neural networks: Evidence from random matrix theory and implications for learning. *Journal of Machine Learning Research*, 22, 2018. URL <https://arxiv.org/abs/1810.01075>.
- B Menze and et al. The multimodal brain tumor image segmentation benchmark (brats). *IEEE Transactions on Medical Imaging*, 34(10):1993–2024, 2015. doi: 10.1109/TMI.2014.2377694.

Sample MNIST Projections

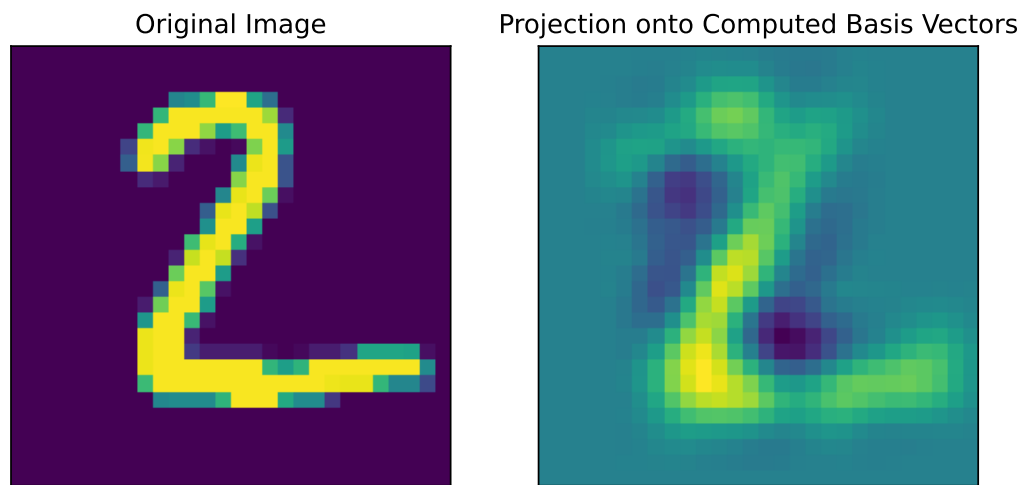


Figure 5: Left: the input image. Right: The projection of the image onto the first 10 singular vectors.

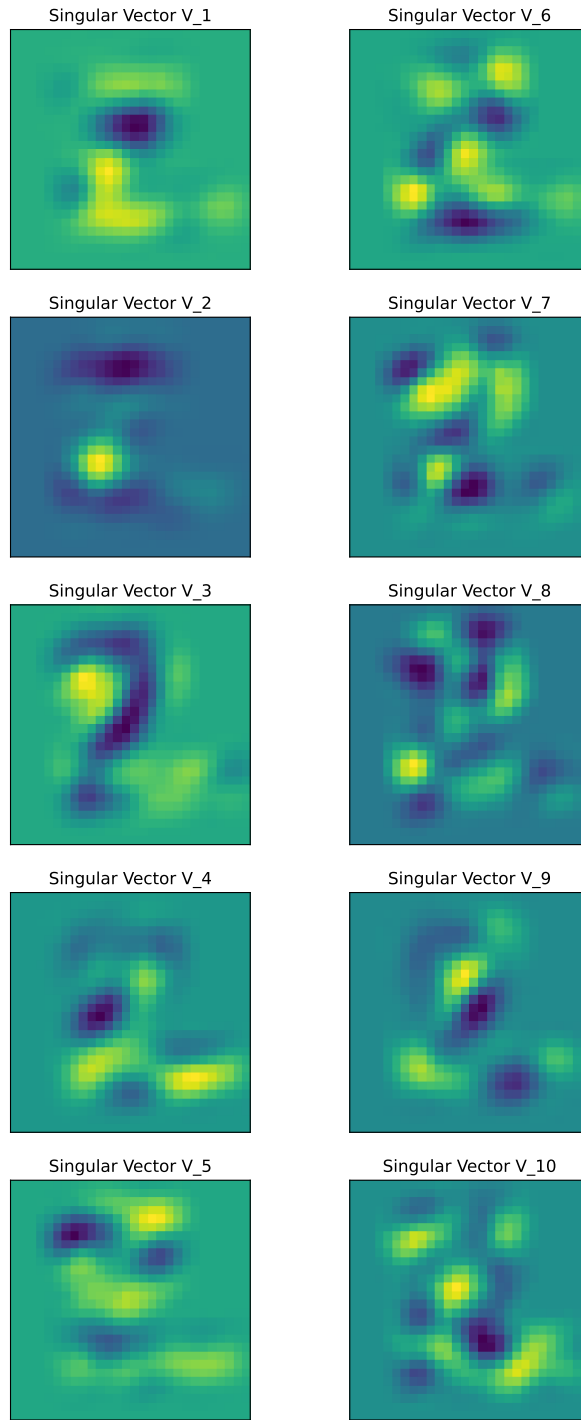


Figure 6: The right singular vectors with respect to the input image in Figure 5.

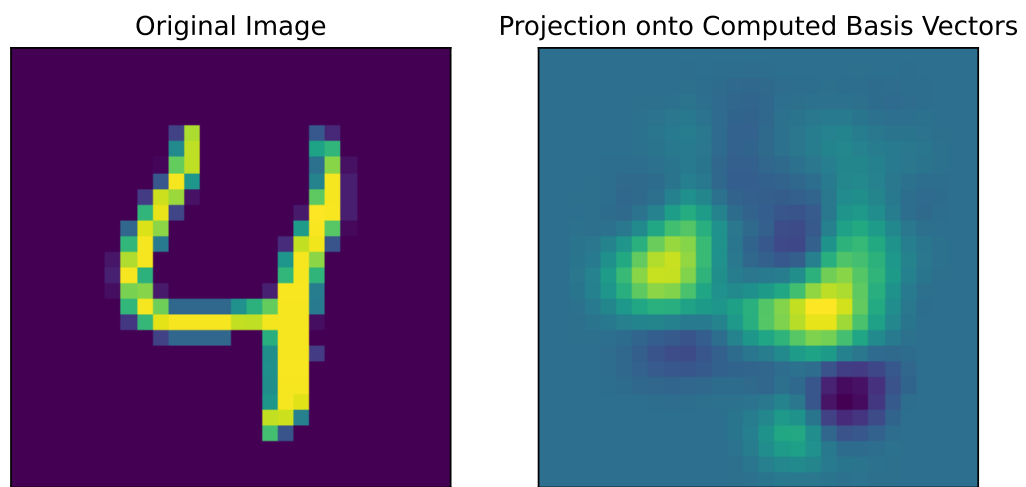


Figure 7: Left: the input image. Right: The projection of the image onto the first 10 singular vectors.

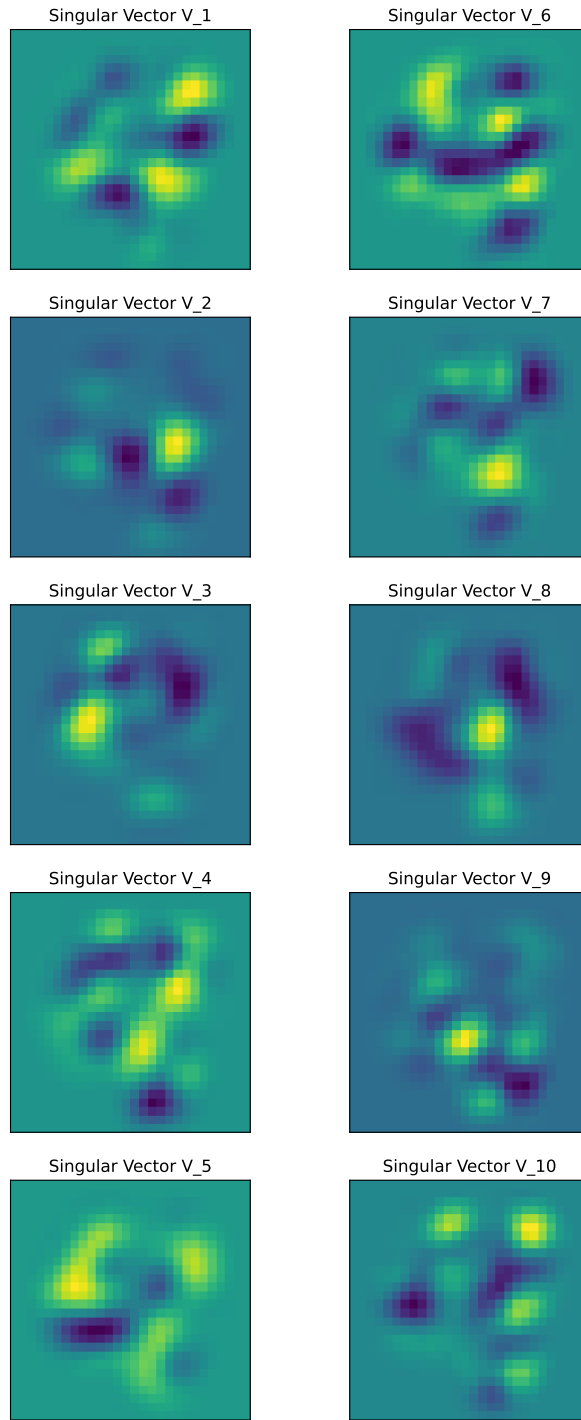


Figure 8: The right singular vectors with respect to the input image in Figure 7.

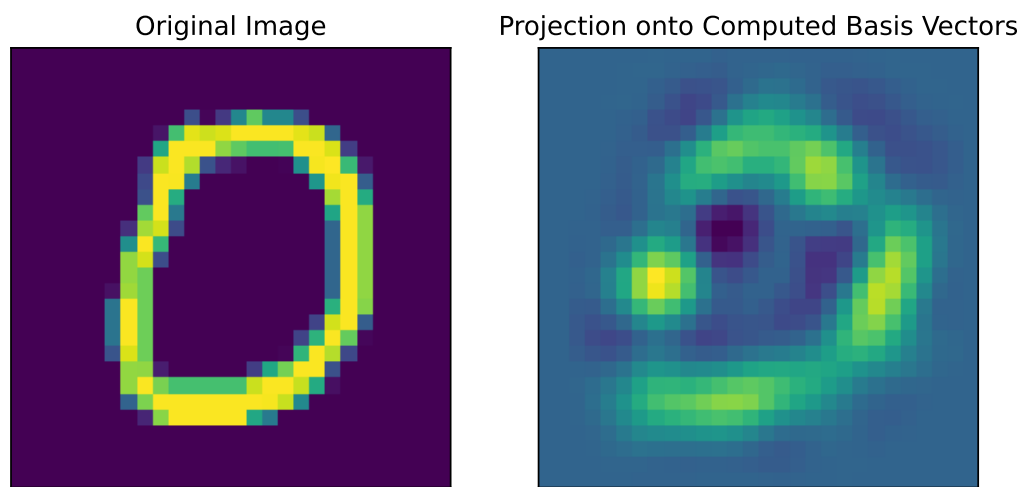


Figure 9: Left: the input image. Right: The projection of the image onto the first 10 singular vectors.

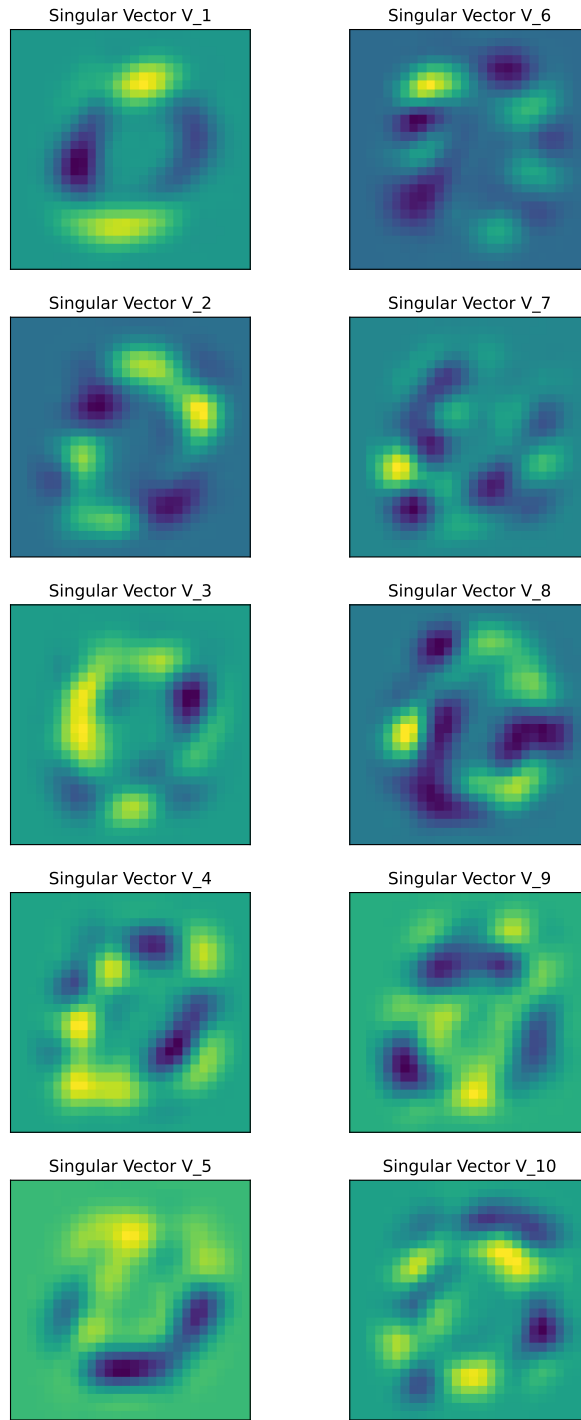


Figure 10: The right singular vectors with respect to the input image in Figure 9.

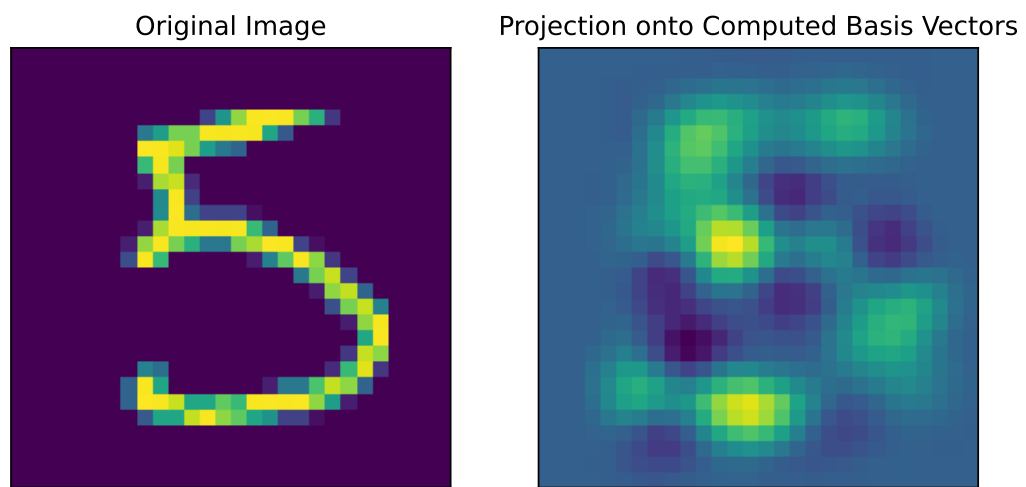


Figure 11: Left: the input image. Right: The projection of the image onto the first 10 singular vectors.

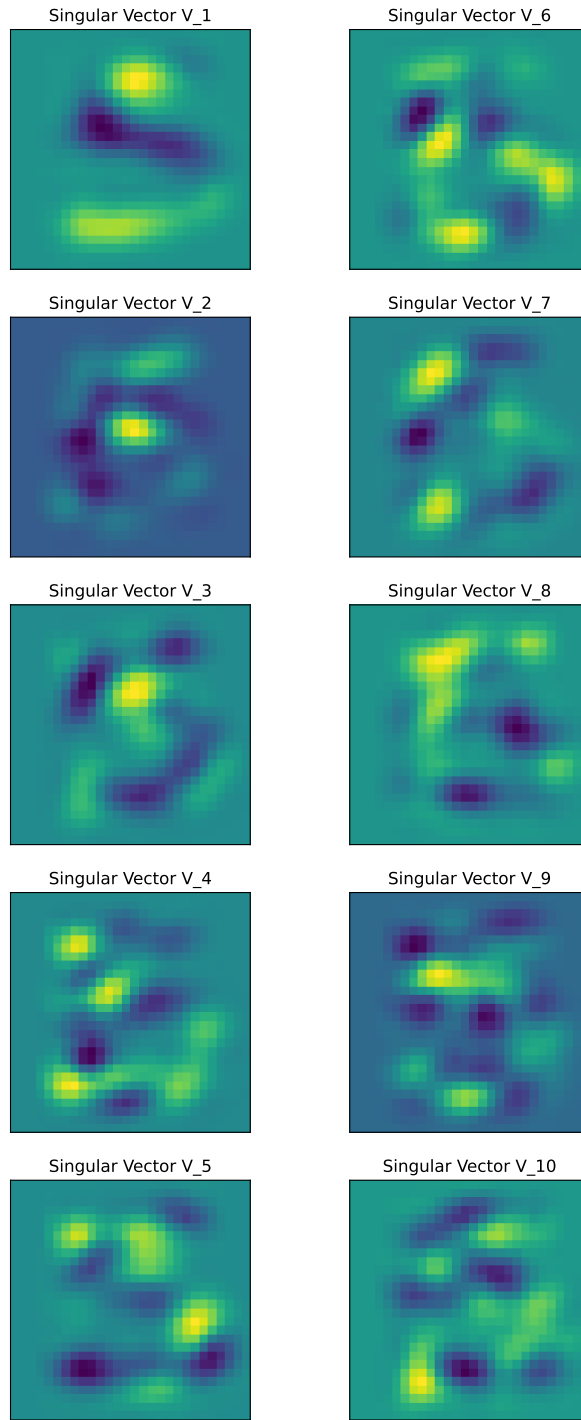


Figure 12: The right singular vectors with respect to the input image in Figure 11.